# Nonlinear Bang-Bang Impact Control for Free Space, Impact and Constrained Motion: Multi-DOF Case

Sang Hoon Kang, Maolin Jin, Pyung H. Chang and Eunjeong Lee, *Member, IEEE*

*Abstract*— **This paper presents stability analysis and experimental results of the nonlinear bang-bang impact controller for multi-degree of freedom robot manipulators. Stability conditions have been derived based on the analysis in $L_\infty^n$ space and their physical interpretation has been given. The analysis shows that the stability of nonlinear bang-bang impact control depends on sampling time and the accuracy of inertia estimation. Stability is enhanced with the decrease of changes in the Coriolis, centrifugal, and disturbance forces. The stability conditions are verified by experiments. Experimental results show that the nonlinear bang-bang impact controller performs a seamless contact manipulation that involves impact with only one control algorithm and the same gains in all three contact modes. It is also shown via experiments that the nonlinear bang-bang impact control is robust to disturbance and environmental changes.**

## I. Introduction

It has been known to be very difficult for robots to interact with a variety of environments including a stiff one with a single simple control algorithm and gain [1]-[3].

In order to address this problem, a nonlinear bang-bang impact control ( NBBIC ) has been proposed by Lee [4]-[6]. Under NBBIC, a robot can successfully interact with an environment without changing control algorithm and control gains. The effectiveness of NBBIC was verified through a set of simulations and experiments [4]-[7].

In this paper, a formal presentation of stability analysis of the nonlinear bang-bang impact control is presented for multi-degree of freedom robotic manipulators. Sufficient stability conditions have been derived based on the analysis in $L_\infty^n$ space and their physical interpretation has been given. Experimental results verify the stability condition. The overall control performance of the NBBIC is demonstrated by experiments in free space, impact, and constrained motion.

This paper is organized as follows: Section II describes the bang-bang impact control along with hybrid Natural Admittance/Time-Delay Control ( NAC/ TDC ). Section III presents the stability analysis of the NBBIC and discusses its physical implications, while Section IV validates the NBBIC stability theorem via experiment and presents the experimental results of NBBIC in free space, contact transition, and constrained motion. Finally, Section V discusses conclusions and suggests future work.

S. H. Kang is with the Mechanical Engineering Department, Korea Advanced Institute of Science and Technology (KAIST), Daejeon, South Korea (corresponding author: +82-42-869-3266; fax: +82-42-869-5226; e-mail: shkang@ mecha.kaist.ac.kr).

M. Jin is with the Mechanical Engineering Department, KAIST. (e-mail: mulan819@kaist.ac.kr).

P. H. Chang is with the Mechanical Engineering Department, KAIST. (e-mail: phchang@kaist.ac.kr).

E. Lee is with the Mechanical Engineering Department, KAIST and was supported by the Brain Korea 21 Project, School of Information Technology, KAIST. (e-mail: eunjeonglee@ieee.org).

## II. Nonlinear Bang-Bang Impact Control

In this section, a brief description of Natural Admittance Control ( NAC ) and Time Delay Control ( TDC ) is presented along with their control laws. Additionally, this section develops NAC/TDC and NBBIC algorithms.

### A. Natural Admittance Control

Under NAC the target dynamics is chosen to be smaller than the maximum target admittance which does not violate the passivity constraint [8]. The simplest form of NAC is

$$\boldsymbol{\tau}(t)=\mathbf{G}_v(\dot{\boldsymbol{\theta}}_{cmd}(t)-\dot{\boldsymbol{\theta}}(t))+\mathbf{K}_{des}\left(\boldsymbol{\theta}_d(t)-\boldsymbol{\theta}(t)\right)+\mathbf{B}_{des}\left(\dot{\boldsymbol{\theta}}_d(t)-\dot{\boldsymbol{\theta}}(t)\right) \quad (1)$$

, where

$$\dot{\boldsymbol{\theta}}_{cmd}(t)=\int\mathbf{M}_s^{-1}\left\{\boldsymbol{\tau}_s+\mathbf{K}_{des}\left(\boldsymbol{\theta}_d(t)-\boldsymbol{\theta}(t)\right)+\mathbf{B}_{des}\left(\dot{\boldsymbol{\theta}}_d(t)-\dot{\boldsymbol{\theta}}(t)\right)\right\}dt \quad (2)$$

$\boldsymbol{\theta}(t)\in\Re^n$ is a joint variable vector. The variable $t$ represents time. $\boldsymbol{\theta}_d(t)\in\Re^n$ and $\dot{\boldsymbol{\theta}}_d(t)\in\Re^n$ are the desired joint position and velocity vectors, respectively. $\boldsymbol{\tau}_s\in\Re^n$ is an external torque vector measured, and $\boldsymbol{\tau}(t)\in\Re^n$ is the control torque vector applied to the joints. $\mathbf{M}_s\in\Re^{n\times n}$, $\mathbf{K}_{des}\in\Re^{n\times n}$, and $\mathbf{B}_{des}\in\Re^{n\times n}$ are the end-point mass, which can be estimated by system identification, and the desired stiffness and damping matrices, respectively. $\mathbf{G}_v\in\Re^{n\times n}$ and $\dot{\boldsymbol{\theta}}_{cmd}(t)\in\Re^n$ represent the diagonal constant velocity feedback gain matrix and the command joint velocity vector, respectively. In (1), the first term corrects deviations of the actual response from the modeled response, $\dot{\boldsymbol{\theta}}_{cmd}$. The second term

is the feedforward term which imposes desired dynamics implicitly. While a robot tries to achieve desired target dynamics, the desired dynamics generate virtual force composed of spring and damping forces on the end effector. Therefore, this virtual force should be accounted for in the force feedback loop through $\dot{\boldsymbol{\theta}}_{\mathbf{cmd}}$. Also, to mask undesirable dynamic effects such as friction, the sensed environment force $\boldsymbol{\tau}_{\mathbf{s}}$ is fed back as a velocity command.

However, like many other interaction controllers, NAC does not achieve the desired performance due to inherent nonlinear dynamics, modeling uncertainties and digital sampling. In order to enhance NAC by compensating the effect of uncertainties via time delay estimation, a hybrid NAC/TDC is developed in the next section.

### B. Hybrid Natural Admittance/Time-Delay Control

The nonlinear dynamics of *n* degree of freedom robots are described by the following dynamic equation.

$$\boldsymbol{\tau}(t)=\mathbf{M}(\boldsymbol{\theta}(t))\ddot{\boldsymbol{\theta}}(t)+\mathbf{V}(\boldsymbol{\theta}(t),\dot{\boldsymbol{\theta}}(t))+\mathbf{G}(\boldsymbol{\theta}(t))+\boldsymbol{\tau}_{\mathbf{s}}(t)+\mathbf{d}(t). \quad (3)$$

where $\mathbf{M}(\boldsymbol{\theta}(t))\in\Re^{n\times n}$ is an inertia matrix, $\mathbf{V}(\boldsymbol{\theta}(t),\dot{\boldsymbol{\theta}}(t))\in\Re^{n}$ is a Coriolis and centrifugal force vector, and $\mathbf{G}(\boldsymbol{\theta}(t))\in\Re^{n}$ is a gravitational force vector. $\mathbf{d}(t)\in\Re^{n}$ is the disturbance vector which includes viscous, Coulomb friction and external disturbances.

Let us define the reference model [9] to achieve an *n* degree of freedom stable 2nd order linear system given by

$$\begin{bmatrix}\dot{\boldsymbol{\theta}}_{\mathbf{r}}(t)\\ \ddot{\boldsymbol{\theta}}_{\mathbf{r}}(t)\end{bmatrix}=\begin{bmatrix}\mathbf{0} & \mathbf{I}\\ \mathbf{c}_{\mathbf{r}} & \mathbf{a}_{\mathbf{r}}\end{bmatrix}\begin{bmatrix}\boldsymbol{\theta}_{\mathbf{r}}(t)\\ \dot{\boldsymbol{\theta}}_{\mathbf{r}}(t)\end{bmatrix}+\begin{bmatrix}\mathbf{0}\\ \mathbf{b}_{\mathbf{r}}\end{bmatrix}\mathbf{r}(t). \quad (4)$$

where $\boldsymbol{\theta}_{\mathbf{r}}(t)\in\Re^{n}$ and $\dot{\boldsymbol{\theta}}_{\mathbf{r}}(t)\in\Re^{n}$ are the reference/desired trajectory vector and its derivative and $\mathbf{r}(t)\in\Re^{n}$ is a reference command vector. $\mathbf{a}_{\mathbf{r}},\mathbf{c}_{\mathbf{r}}\in\Re^{n\times n}$ and $\mathbf{b}_{\mathbf{r}}\in\Re^{n\times n}$ are constant diagonal matrices for the reference model. For a stable reference system, $\mathbf{a}_{\mathbf{r}}$ and $\mathbf{c}_{\mathbf{r}}$ are selected to be negative definite matrices. If the range of robot inertia $\mathbf{M}(\boldsymbol{\theta}(t))$ is known, the following TDC law is derived to achieve the desired dynamics of the reference model of (4) by using time delay estimation [9]-[10]. *L* is a small time-delay and can be regarded as a sampling time.

$$\begin{aligned}\boldsymbol{\tau}(t)=\bar{\mathbf{M}}\big[&\mathbf{c}_{\mathbf{r}}\boldsymbol{\theta}(t)+\mathbf{a}_{\mathbf{r}}\dot{\boldsymbol{\theta}}(t)+\mathbf{b}_{\mathbf{r}}\mathbf{r}(t)-\mathbf{K}_{\mathbf{p}}\mathbf{e}(t)-\mathbf{K}_{\mathbf{d}}\dot{\mathbf{e}}(t)\big]\\ &-\bar{\mathbf{M}}\ddot{\boldsymbol{\theta}}(t-L)+\boldsymbol{\tau}(t-L)\end{aligned}, \quad (5)$$

where $\mathbf{e}(t),\dot{\mathbf{e}}(t)\in\Re^{n}$ are position error ($\mathbf{e}(t)=\boldsymbol{\theta}_{\mathbf{r}}(t)-\boldsymbol{\theta}(t)$) and its derivative and $\mathbf{K}_{\mathbf{p}},\mathbf{K}_{\mathbf{d}}\in\Re^{n\times n}$ are constant diagonal matrices for the position and velocity error vectors, respectively. $\bar{\mathbf{M}}\in\Re^{n\times n}$ is a constant matrix representing the inertia estimate.

If we compare the NAC law of (1) and (2) to the TDC control law of (5), the velocity command vector term $\dot{\boldsymbol{\theta}}_{\mathbf{cmd}}$ can be regarded as a reference input, $\mathbf{r}$, in the time delay control law. The NAC stiffness and damping terms are essentially the position and velocity error terms in TDC, respectively. Therefore, if we set $\boldsymbol{\theta}_{\mathbf{d}}=\boldsymbol{\theta}_{\mathbf{r}}$, $\mathbf{r}=\dot{\boldsymbol{\theta}}_{\mathbf{cmd}}$, $-\mathbf{a}_{\mathbf{r}}=\mathbf{b}_{\mathbf{r}}=\mathbf{G}_{\mathbf{v}}$, $\mathbf{K}_{\mathbf{des}}=\mathbf{K}_{\mathbf{P}}$ and $\mathbf{B}_{\mathbf{des}}=\mathbf{K}_{\mathbf{d}}$, we can nest the NAC loop inside the TDC loop. Thereby, the hybrid NAC/TDC law becomes [4]-[7].

$$\begin{aligned}\boldsymbol{\tau}(t)=\bar{\mathbf{M}}\big[&\mathbf{G}_{\mathbf{v}}(\dot{\boldsymbol{\theta}}_{\mathbf{cmd}}(t)-\dot{\boldsymbol{\theta}}(t))+\mathbf{K}_{\mathbf{des}}(\boldsymbol{\theta}_{\mathbf{d}}(t)-\boldsymbol{\theta}(t))\\ &+\mathbf{B}_{\mathbf{des}}(\dot{\boldsymbol{\theta}}_{\mathbf{d}}(t)-\dot{\boldsymbol{\theta}}(t))+\mathbf{c}_{\mathbf{r}}\boldsymbol{\theta}(t)\big]-\bar{\mathbf{M}}\ddot{\boldsymbol{\theta}}(t-L)+\boldsymbol{\tau}(t-L)\end{aligned} \quad (6)$$

In order to implement the control law only one system parameter, the inertia, needs to be estimated.

### C. Nonlinear Bang-Bang Impact Control

Even though the NAC/TDC yields good control performance during free and constrained motion, its performance is limited when a robot experiences impact. Therefore, a nonlinear bang-bang impact controller is proposed to enhance the impact behavior of robots by using the NAC/TDC. The control strategy can be summarized as follows. During free-space motion, NAC/TDC is used. During impact transient when contact is broken due to bouncing, no control input is applied; and when contact is made, NAC/TDC is used. NAC/TDC is used again after contact is established. NAC/TDC also brings a robot back into contact with an environment when it stops in free space due to the zero control input during contact transient. This incident occurs if the restoring spring force cannot overcome friction and inertia of the robot under no control action after it bounces off from the environment. The resulting control strategy for a multi-input multi-output ( MIMO ) system is described as follows.

1) Unconstrained Motion: NAC/TDC
   If $|\mathbf{F}_{\mathbf{s}}|<F_{impact}$ then NAC/TDC (7)
2) In contact Transition: Bang-Bang Control
   a) If the robot is in contact with the environment ($|\mathbf{F}_{\mathbf{s}}|>F_{sw}$), then NAC/TDC (8)
   b) If the robot is out of contact ($|\mathbf{F}_{\mathbf{s}}|<F_{sw}$), then $\boldsymbol{\tau}(t)=0$ (9)
   c) If $|\mathbf{F}_{\mathbf{s}}|<F_{sw}$ and $|\mathbf{v}(t)|<v_{threshold}$, then NAC/TDC (10)
3) After Impact Transient: NAC/TDC
   If $|\mathbf{F}_{\mathbf{s}}|>F_{sw}$, then NAC/TDC (11)

$\mathbf{F}_{\mathbf{s}}\in\Re^{n}$ and $\mathbf{v}(t)\in\Re^{n}$ are measured external force and velocity in Cartesian space, respectively. $F_{impact}\in\Re$, $F_{sw}\in\Re$ and $v_{threshold}\in\Re$ are threshold values to detect impact, switching and zero velocity, respectively, and are dependent on the sensitivity of the torque and position sensors. These values should be zero ideally, but they have certain threshold values in reality due to experimental noises. The NBBIC is very effective since it makes robots naturally dissipate their impact energy after they bounce off from the environment rather than exert excessive control input to reject impact

disturbance.

## III. Stability Analysis of Nonlinear Bang-Bang Impact Control

To derive stability condition, we assume that the robot and environment have finite stiffness and thus impact force has finite magnitude and finite duration. We further assume that during the short time interval of collision, the joint position of a robotic system remains unchanged and joint velocities are finite [11]-[15].

We do not model impact force as a Dirac delta function which has infinite magnitude and infinitesimally short duration [12],[14] because the colliding robot and the environment are not perfect rigid bodies with infinite stiffness. Therefore, there is *no discontinuity,* such as instantaneous jump of states, in dynamic equations of our impact model

### A. Grouping of Each Control Stage

For stability analysis, the five stages of the nonlinear bang-bang impact control of (7)-(11) have been categorized into three groups in table 1 according to their physical characteristics and contact mode. Note that the initial conditions of the errors are not zero in all cases. The stability analysis was performed for each group separately. The stability condition for the transition from one group to the next can be derived from that of the next group it switched to by setting nonzero initial condition.

### B. NAC/TDC Error-ε inequality

In order to derive the stability condition of NBBIC, we first have to establish the general inequality for NAC/TDC. The nonlinear dynamics of (3) for *n* degree of freedom robot can be divided into two terms, the known term and the unknown and/or uncertain nonlinear dynamics terms represented by $\mathbf{H}(t)\in\Re^n$ as below.

$$\boldsymbol{\tau}(t)=\bar{\mathbf{M}}\ddot{\boldsymbol{\theta}}(t)+\mathbf{H}(t) \quad ,(12)$$

where

$$\mathbf{H}(t)=\left(\mathbf{M}(\boldsymbol{\theta}(t))-\bar{\mathbf{M}}\right)\ddot{\boldsymbol{\theta}}(t)+\mathbf{V}(\boldsymbol{\theta}(t),\dot{\boldsymbol{\theta}}(t))+\mathbf{G}(\boldsymbol{\theta}(t))+\mathbf{d}(t)+\boldsymbol{\tau}_s(t) \quad (13)$$

Likewise, the NAC/TDC of (6) can be described as follows.

$$\boldsymbol{\tau}(t)=\bar{\mathbf{M}}\mathbf{u}(t)+\mathbf{H}(t-L) \quad .(14)$$

where

TABLE I
GROUPING OF CONTROL STAGE

| Group | Characteristics | | Case |
|---|---|---|---|
| | Physical Characteristics | Mode | |
| Group 1 | - Before Contact<br>- No external force | Free space - 1 | 1<br>2-c |
| Group 2 | - Nonzero external force | Constrained space | 2-a,3 |
| Group 3 | - Out of contact<br>- No external force | Free space - 2 | 2-b |
| | $\mathbf{e}(0)\neq 0,\dot{\mathbf{e}}(0)\neq 0,\ddot{\mathbf{e}}(0)\neq 0$ | | All cases |

$$\begin{aligned}\mathbf{u}(t) &= \mathbf{G}_v\left(\dot{\boldsymbol{\theta}}_{cmd}(t)-\dot{\boldsymbol{\theta}}(t)\right)+\mathbf{K}_{des}\left(\boldsymbol{\theta}_d(t)-\boldsymbol{\theta}(t)\right)\\ &\quad+\mathbf{B}_{des}\left(\dot{\boldsymbol{\theta}}_d(t)-\dot{\boldsymbol{\theta}}(t)\right)+\mathbf{c}_r\boldsymbol{\theta}(t)\end{aligned} \quad ,(15)$$

where

$$\dot{\boldsymbol{\theta}}_{cmd}(t)=\int\mathbf{M}_s^{-1}\left\{\boldsymbol{\tau}_s+\mathbf{K}_{des}\left(\boldsymbol{\theta}_d(t)-\boldsymbol{\theta}(t)\right)+\mathbf{B}_{des}\left(\dot{\boldsymbol{\theta}}_d(t)-\dot{\boldsymbol{\theta}}(t)\right)\right\}dt \quad (16)$$

Subtracting (14) from (12) yields,

$$\bar{\mathbf{M}}\left(\mathbf{u}(t)-\ddot{\boldsymbol{\theta}}(t)\right)=\mathbf{H}(t)-\mathbf{H}(t-L) \quad (17)$$

If we set

$$\boldsymbol{\varepsilon}(t)\equiv\mathbf{u}(t)-\ddot{\boldsymbol{\theta}}(t) \quad ,(18)$$

then (17) can be written as below.

$$\boldsymbol{\varepsilon}(t)=\bar{\mathbf{M}}^{-1}\left(\mathbf{H}(t)-\hat{\mathbf{H}}(t)\right)=\bar{\mathbf{M}}^{-1}\left(\mathbf{H}(t)-\mathbf{H}(t-L)\right) \quad (19)$$

$\boldsymbol{\varepsilon}(t)\in\Re^n$ is an estimation error vector between the nonlinear dynamics $\mathbf{H}(t)$ and the estimated nonlinear dynamics $\hat{\mathbf{H}}(t)$. $\hat{\mathbf{H}}(t)$ is estimated by using $\mathbf{H}(t-L)$, the value of nonlinear dynamics at time *t-L*.

The substitution of (15) and (16) into (18) and mathematical manipulation yields the following error dynamics. The mathematical manipulation does not necessitate the initial value of $\dot{\boldsymbol{\theta}}_{cmd}$.

$$\begin{aligned}&\mathbf{M}_s^{-1}\mathbf{G}_v\mathbf{K}_{des}\int\mathbf{e}(t)dt+\left(\mathbf{M}_s^{-1}\mathbf{G}_v\mathbf{B}_{des}+\mathbf{K}_{des}-\mathbf{c}_r\right)\mathbf{e}(t)\\ &+\left(\mathbf{G}_v+\mathbf{B}_{des}\right)\dot{\mathbf{e}}(t)+\ddot{\mathbf{e}}(t)\\ &=\boldsymbol{\varepsilon}(t)-\mathbf{c}_r\boldsymbol{\theta}_d(t)+\ddot{\boldsymbol{\theta}}_d(t)+\mathbf{G}_v\dot{\boldsymbol{\theta}}_d(t)-\mathbf{M}_s^{-1}\mathbf{G}_v\int\boldsymbol{\tau}_s dt\end{aligned} \quad .(20)$$

where $\mathbf{e}(t)=\boldsymbol{\theta}_d(t)-\boldsymbol{\theta}(t)$. Equation (20) describes the time-delay estimation error $\boldsymbol{\varepsilon}(t)$ in terms of the desired trajectories and the errors between the desired trajectories and the actual plant states and their derivatives.

***Lemma1.Error-ε Inequality:*** In the case of *n* degree of freedom robot under NAC/TDC in constrained space, if the desired trajectory and its derivatives are in $L_\infty^n$ space and the external force $\boldsymbol{\tau}_s$ is in $L_\infty^n$ space, i.e., $\boldsymbol{\theta}_d,\dot{\boldsymbol{\theta}}_d,\ddot{\boldsymbol{\theta}}_d\in L_\infty^n$, and $\boldsymbol{\tau}_s\in L_\infty^n$, then the following inequalities can be obtained. In the case of impact, $\boldsymbol{\tau}_s\in L_\infty^n$ holds because $\|\boldsymbol{\tau}_s\|_\infty=\|\delta_a(t)\|_\infty=1/2a$. $\delta_a(t)$ is the unit pulse function[1].

$$\begin{aligned}\|\mathbf{e}\|_{T\infty}&\le\beta_1\|\boldsymbol{\varepsilon}\|_{T\infty}+\gamma_1\|\boldsymbol{\tau}_s\|_{T\infty}+\eta_1\|\boldsymbol{\theta}_d\|_{T\infty}+\rho_1\\ \|\dot{\mathbf{e}}\|_{T\infty}&\le\beta_2\|\boldsymbol{\varepsilon}\|_{T\infty}+\gamma_2\|\boldsymbol{\tau}_s\|_{T\infty}+\eta_2\|\dot{\boldsymbol{\theta}}_d\|_{T\infty}+\rho_2\\ \|\ddot{\mathbf{e}}\|_{T\infty}&\le\beta_3\|\boldsymbol{\varepsilon}\|_{T\infty}+\gamma_3\|\boldsymbol{\tau}_s\|_{T\infty}+\eta_3\|\ddot{\boldsymbol{\theta}}_d\|_{T\infty}+\rho_3\\ \|\tilde{\mathbf{e}}_I\|_{T\infty}&\le\beta_4\|\boldsymbol{\varepsilon}\|_{T\infty}+\gamma_4\|\boldsymbol{\tau}_s\|_{T\infty}+\eta_4\|\boldsymbol{\theta}_d\|_{T\infty}+\rho_4\\ \|\tilde{\mathbf{e}}\|_{T\infty}&\le\beta_5\|\boldsymbol{\varepsilon}\|_{T\infty}+\gamma_5\|\boldsymbol{\tau}_s\|_{T\infty}+\eta_5\|\boldsymbol{\theta}_d\|_{T\infty}+\rho_5\\ \|\ddot{\mathbf{e}}\|_{T\infty}&\le\beta_6\|\boldsymbol{\varepsilon}\|_{T\infty}+\gamma_6\|\boldsymbol{\tau}_s\|_{T\infty}+\eta_6\|\dot{\boldsymbol{\theta}}_d\|_{T\infty}+\rho_6\end{aligned} \quad .(21)$$

where $\mathbf{e}_I$ is the time integral of error. $\beta_i,\gamma_i,\eta_i$ are $L_\infty^n$ gains of

[1] $\|\bullet\|_{T\infty}$ denotes truncated $L_\infty^n$ norm of $\bullet(t)$

operator $\mathbf{H}_i, \mathbf{G}_i, \mathbf{R}_i$ ( $i = 1 \cdots 6$ ) and $\mathbf{H}_i, \mathbf{G}_i$ and $\mathbf{R}_i$ are operators as below.

$$\begin{array}{lll} \mathbf{H}_1 : \boldsymbol{\varepsilon} \mapsto \mathbf{e} & \mathbf{G}_1 : \boldsymbol{\tau}_s \mapsto \mathbf{e} & \mathbf{R}_1 : \boldsymbol{\theta}_d \mapsto \mathbf{e} \\ \mathbf{H}_2 : \boldsymbol{\varepsilon} \mapsto \dot{\mathbf{e}} & \mathbf{G}_2 : \boldsymbol{\tau}_s \mapsto \dot{\mathbf{e}} & \mathbf{R}_2 : \dot{\boldsymbol{\theta}}_d \mapsto \dot{\mathbf{e}} \\ \mathbf{H}_3 : \boldsymbol{\varepsilon} \mapsto \ddot{\mathbf{e}} & \mathbf{G}_3 : \boldsymbol{\tau}_s \mapsto \ddot{\mathbf{e}} & \mathbf{R}_3 : \ddot{\boldsymbol{\theta}}_d \mapsto \ddot{\mathbf{e}} \\ \mathbf{H}_4 : \boldsymbol{\varepsilon} \mapsto \tilde{\mathbf{e}}_l & \mathbf{G}_4 : \boldsymbol{\tau}_s \mapsto \tilde{\mathbf{e}}_l & \mathbf{R}_4 : \boldsymbol{\theta}_d \mapsto \tilde{\mathbf{e}}_l \\ \mathbf{H}_5 : \boldsymbol{\varepsilon} \mapsto \tilde{\dot{\mathbf{e}}} & \mathbf{G}_5 : \boldsymbol{\tau}_s \mapsto \tilde{\dot{\mathbf{e}}} & \mathbf{R}_5 : \dot{\boldsymbol{\theta}}_d \mapsto \tilde{\dot{\mathbf{e}}} \\ \mathbf{H}_6 : \boldsymbol{\varepsilon} \mapsto \tilde{\ddot{\mathbf{e}}} & \mathbf{G}_6 : \boldsymbol{\tau}_s \mapsto \tilde{\ddot{\mathbf{e}}} & \mathbf{R}_6 : \ddot{\boldsymbol{\theta}}_d \mapsto \tilde{\ddot{\mathbf{e}}} \end{array} \quad (22)$$

$\rho_i$ $(i = 1 \cdots 6)$ is a constant related to the initial condition of errors.

***Proof of Lemma 1:*** First, we can obtain stable transfer function matrices between the error and ε, the error and external torque, and the error and desired trajectory by using proper control gains. Then, it can be said that initial condition related parts exponentially converge and are bounded. Second, the stable transfer function has finite $L_\infty^n$ gains $\beta_i, \gamma_i, \eta_i$ $(i = 1 \cdots 6)$. Thus (21) is obtained. □

***Remark 1:*** $\beta_5$ and $\beta_6$ are $L_\infty^n$ gains of the time differences of impulse response matrix $\mathbf{H}_1$ and matrix $\mathbf{H}_2$, respectively. If time delay $L$ is small enough, $\beta_5$ and $\beta_6$ are also small.

### C. ε- $L_\infty^n$ Norm Bound

In this section, $L_\infty^n$ upper bound of $\boldsymbol{\varepsilon}$ is derived based on the grouping in table 1. The analysis for the free space case of group 1 is presented first.

Substituting (6), (15) and (18) into (3) yields the following equation[2] [10].

$$\begin{aligned} \boldsymbol{\varepsilon}(t) = & \left(\mathbf{I} - \mathbf{M}^{-1}(t)\bar{\mathbf{M}}\right)\tilde{\mathbf{u}}(t) + \left(\mathbf{I} - \mathbf{M}^{-1}(t)\bar{\mathbf{M}}\right)\boldsymbol{\varepsilon}(t-L) \\ & + \mathbf{M}^{-1}(t)\Big[\tilde{\mathbf{M}}(t)\left(-\ddot{\mathbf{e}}(t-L) + \ddot{\boldsymbol{\theta}}_d(t-L)\right) \\ & + \tilde{\mathbf{V}}(t) + \tilde{\mathbf{G}}(t) + \tilde{\boldsymbol{\tau}}_s(t)\Big] \end{aligned} \quad (23)$$

For derivation of Lemma 2-1 and 2-2, new variables are defined as follow.

$$\begin{array}{ll} \tilde{\mathbf{M}}(t) = \mathbf{M}(t) - \mathbf{M}(t-L), & \mathbf{Q}(t) = \mathbf{V}(t) + \mathbf{d}(t), \\ \Delta \equiv \mathbf{I} - \mathbf{M}^{-1}(t)\bar{\mathbf{M}}, & \tilde{\mathbf{Q}}(t) = \mathbf{Q}(t) - \mathbf{Q}(t-L) \end{array} \quad (24)$$

$\mathbf{Q}(t) \in \Re^n$ contains Coriolis and centrifugal forces and disturbances. During the infinitesimally short time interval of collision, the joint position of a robotic system remains unchanged and joint velocities are finite [13], [15]. Accordingly, Coriolis and centrifugal terms remain finite upon impact. Thus $\tilde{\mathbf{Q}}(t)$ is bounded.

To derive stability conditions, we assume a compact set as

$$S = \left\{ \mathbf{e}(t), \dot{\mathbf{e}}(t) \in \Re^n \,\middle|\, \|\mathbf{e}(t)\|_\infty^2 \le D_1, \|\dot{\mathbf{e}}(t)\|_\infty^2 \le D_2 \right\} \quad (25)$$

with constants $D_1 > 0$ and $D_2 > 0$. Then, we can make the terms for Coriolis, centrifugal forces and disturbances have the following relationship [16], [17].

$$\mathbf{Q}(t) = \mathbf{Q}_d(t) + \mathbf{O}_q\left(\mathbf{e}(t), \dot{\mathbf{e}}(t)\right) + \mathbf{w}(t) \quad (26)$$

$$\mathbf{O}_q\left(t\right) \cong \mathbf{q}_1(t)\dot{\mathbf{e}}(t) + \mathbf{q}_2(t)\mathbf{e}(t) \quad (27)$$

,where $\mathbf{Q}_d(t) = \mathbf{Q}(\boldsymbol{\theta}_d(t), \dot{\boldsymbol{\theta}}_d(t))$ and $\mathbf{q}_1(t), \mathbf{q}_2(t) \in \Re^n$ are bounded functions of time. $\mathbf{w}(t) \in \Re^n$ includes external disturbances and frictions. In other words, if we assume that there always exists the set *S* within which the position and velocity errors are guaranteed to be bounded, then eq. (27) can be always satisfied [ Appendix ].

***Lemma 2-1. ε- $L_\infty^n$ Norm Bound Inequality (Free space case):*** In the case of *n* degree of freedom robot under NAC/TDC in free space, if the desired trajectory and its derivatives are in $L_\infty^n$ space and the time difference of uncertainty including disturbance is also in $L_\infty^n$ space, i.e., $\boldsymbol{\theta}_d, \dot{\boldsymbol{\theta}}_d, \ddot{\boldsymbol{\theta}}_d \in L_\infty^n$ and $\tilde{\mathbf{w}} \in L_\infty^n$, then the following inequality can be obtained.

$$\left(1 - \mu - \delta_1\beta_4 - \delta_2\beta_5 - \delta_3\beta_6 - \delta_4\beta_1 - \delta_5\beta_2 - \delta_6\beta_3\right)\|\boldsymbol{\varepsilon}\|_{T\infty} \le \psi_{G1} \quad .$$

where

$$\begin{aligned} \mu &= \left\| \|\boldsymbol{\Delta}\|_{i2} \right\|_\infty \\ \delta_1 &= \left\| \|\boldsymbol{\Delta}\mathbf{G}_v\mathbf{M}_s^{-1}\mathbf{K}_{des}\|_{i2} \right\|_\infty \\ \delta_2 &= \left\| \|\boldsymbol{\Delta}\left(\mathbf{G}_v\mathbf{M}_s^{-1}\mathbf{B}_{des} + \mathbf{K}_{des} - \mathbf{c}_r\right) + \mathbf{M}^{-1}(t)\mathbf{q}_2(t)\|_{i2} \right\|_\infty \\ \delta_3 &= \left\| \|\boldsymbol{\Delta}\left(\mathbf{G}_v + \mathbf{B}_{des}\right) + \mathbf{M}^{-1}(t)\mathbf{q}_1(t)\|_{i2} \right\|_\infty \\ \delta_4 &= \left\| \|\mathbf{M}^{-1}(t)\tilde{\mathbf{q}}_2(t)\|_{i2} \right\|_\infty \\ \delta_5 &= \left\| \|\mathbf{M}^{-1}(t)\tilde{\mathbf{q}}_1(t)\|_{i2} \right\|_\infty \\ \delta_6 &= \left\| \|\mathbf{M}^{-1}(t)\tilde{\mathbf{M}}(t)\|_{i2} \right\|_\infty \\ \psi_{G1} &= \Big\| \boldsymbol{\Delta}\mathbf{c}_r\tilde{\boldsymbol{\theta}}_d(t) - \boldsymbol{\Delta}\mathbf{G}_v\tilde{\dot{\boldsymbol{\theta}}}_d(t) \\ &\quad + \mathbf{M}^{-1}(t)(\tilde{\mathbf{M}}(t)\ddot{\boldsymbol{\theta}}_d(t-L) + \tilde{\mathbf{Q}}_d(t) + \tilde{\mathbf{G}}(t) + \tilde{\mathbf{w}}(t)) \Big\|_\infty \\ &\quad + \delta_1\left(\eta_4\|\boldsymbol{\theta}_d(t)\|_{T\infty} + \rho_4\right) + \delta_2\left(\eta_5\|\boldsymbol{\theta}_d(t)\|_{T\infty} + \rho_5\right) \\ &\quad + \delta_3\left(\eta_6\|\dot{\boldsymbol{\theta}}_d(t)\|_{T\infty} + \rho_6\right) + \delta_4\left(\eta_1\|\boldsymbol{\theta}_d(t)\|_{T\infty} + \rho_1\right) \\ &\quad + \delta_5\left(\eta_2\|\dot{\boldsymbol{\theta}}_d(t)\|_{T\infty} + \rho_2\right) + \delta_6\left(\eta_3\|\ddot{\boldsymbol{\theta}}_d(t)\|_{T\infty} + \rho_3\right) \end{aligned} \quad (28)$$

***Proof of Lemma 2-1:*** The symbol $\Delta, \mathbf{M}(t) \in \Re^{n \times n}$ and $\mathbf{G}(t) \in \Re^{n \times n}$ are sine and/or cosine functions of joint angles and thus they are bounded. $\tilde{\mathbf{M}} \in \Re^{n \times n}$ and $\tilde{\mathbf{G}} \in \Re^n$ are also bounded because they are the difference of bounded functions between time *t* and *t*-*L*.

Substituting (15), (16), (24) and (27) into (23) yields the following.

$$\begin{aligned} \boldsymbol{\varepsilon}(t) = & \boldsymbol{\Delta}\boldsymbol{\varepsilon}(t-L) + \boldsymbol{\Delta}\mathbf{G}_v\mathbf{M}_s^{-1}\mathbf{K}_{des}\tilde{\mathbf{e}}_l(t) \\ & + \left(\boldsymbol{\Delta}\left(\mathbf{G}_v\mathbf{M}_s^{-1}\mathbf{B}_{des} + \mathbf{K}_{des} - \mathbf{c}_r\right) + \mathbf{M}^{-1}(t)\mathbf{q}_2(t)\right)\tilde{\mathbf{e}}(t) \\ & + \left(\boldsymbol{\Delta}\left(\mathbf{G}_v + \mathbf{B}_{des}\right) + \mathbf{M}^{-1}(t)\mathbf{q}_1(t)\right)\tilde{\dot{\mathbf{e}}}(t) \\ & + \left(\mathbf{M}^{-1}(t)\tilde{\mathbf{q}}_2\right)\mathbf{e}(t-L) + \left(\mathbf{M}^{-1}(t)\tilde{\mathbf{q}}_1\right)\dot{\mathbf{e}}(t-L) \\ & - \left(\mathbf{M}^{-1}(t)\tilde{\mathbf{M}}(t)\right)\ddot{\mathbf{e}}(t-L) + \boldsymbol{\Delta}\mathbf{c}_r\tilde{\boldsymbol{\theta}}_d(t) - \boldsymbol{\Delta}\mathbf{G}_v\tilde{\dot{\boldsymbol{\theta}}}_d(t) \\ & + \mathbf{M}^{-1}(t)(\tilde{\mathbf{M}}(t)\ddot{\boldsymbol{\theta}}_d(t-L) + \tilde{\mathbf{Q}}_d(t) + \tilde{\mathbf{G}}(t) + \tilde{\mathbf{w}}(t)) \end{aligned} \quad (29)$$

[2] $\tilde{\bullet}$ denotes $\bullet(t) - \bullet(t-L)$.

Take norms of both sides of (29). Define each term $\mu$ and $\delta_i (i=1\cdots 6)$ as in (28), and $\psi_{1\_G1}$ as below.

$$\begin{aligned}\psi_{1\_G1} = \Big\| & \Delta\mathbf{c}_r\tilde{\boldsymbol{\theta}}_d(t) - \Delta\mathbf{G}_v\dot{\tilde{\boldsymbol{\theta}}}_d(t) \\ & + \mathbf{M}^{-1}(t)(\tilde{\mathbf{M}}(t)\ddot{\boldsymbol{\theta}}_d(t-L) + \tilde{\mathbf{Q}}_d(t) + \tilde{\mathbf{G}}(t) + \tilde{\mathbf{w}}(t))\Big\|_\infty\end{aligned} \quad (30)$$

Then we can derive the following inequality.

$$\begin{aligned}\|\boldsymbol{\varepsilon}(t)\|_{T\infty} \le & \big(\mu\|\boldsymbol{\varepsilon}(t-L)\|_{T\infty} + \delta_1\|\tilde{\mathbf{e}}_l(t)\|_{T\infty} + \delta_2\|\tilde{\mathbf{e}}(t)\|_{T\infty} \\ & + \delta_3\|\dot{\tilde{\mathbf{e}}}(t)\|_{T\infty} + \delta_4\|\mathbf{e}(t-L)\|_{T\infty} \\ & + \delta_5\|\dot{\mathbf{e}}(t-L)\|_{T\infty} + \delta_6\|\ddot{\mathbf{e}}(t-L)\|_{T\infty} + \psi_{1\_G1}\big)\end{aligned} \quad (31)$$

From (28) and Lemma 1, we get[3]

$$\begin{aligned}\|\boldsymbol{\varepsilon}(t)\|_{T\infty} \le & \mu\|\boldsymbol{\varepsilon}(t)\|_{T\infty} + \delta_1\beta_4\|\boldsymbol{\varepsilon}(t)\|_{T\infty} + \delta_2\beta_5\|\boldsymbol{\varepsilon}(t)\|_{T\infty} \\ & + \delta_3\beta_6\|\boldsymbol{\varepsilon}(t)\|_{T\infty} + \delta_4\beta_1\|\boldsymbol{\varepsilon}(t)\|_{T\infty} + \delta_5\beta_2\|\boldsymbol{\varepsilon}(t)\|_{T\infty} \\ & + \delta_6\beta_3\|\boldsymbol{\varepsilon}(t)\|_{T\infty} + \psi_{G1}\end{aligned} \quad (32)$$

Rearranging (32) leads to,

$$(1-\mu-\delta_1\beta_4-\delta_2\beta_5-\delta_3\beta_6-\delta_4\beta_1-\delta_5\beta_2-\delta_6\beta_3)\|\boldsymbol{\varepsilon}\|_{T\infty} \le \psi_{G1} \quad (33)$$

Note that $\psi_{1\_G1}$ and $\psi_{G1}$ consist of bounded values. □

Similarly, for the constrained space case of group 2 Lemma 2-2 can be obtained as below. The only difference is that there exists an external force in the constrained space case. ( Proof can be available upon request. )

***Lemma 2-2. ε- $L_\infty^n$ Norm Bound Inequality (Constrained Space Case):*** In the case of $n$ degree of freedom robot under NAC/TDC in constrained space, if the desired trajectory and its derivatives are in $L_\infty^n$ space and the external force and the time difference of uncertainty including disturbance are also in $L_\infty^n$ space, i.e., $\boldsymbol{\theta}_d, \dot{\boldsymbol{\theta}}_d, \ddot{\boldsymbol{\theta}}_d \in L_\infty^n$, $\boldsymbol{\tau}_s \in L_\infty^n$ and $\tilde{\mathbf{w}} \in L_\infty^n$, then the following inequality can be obtained.

$$(1-\mu-\delta_1\beta_4-\delta_2\beta_5-\delta_3\beta_6-\delta_4\beta_1-\delta_5\beta_2-\delta_6\beta_3)\|\boldsymbol{\varepsilon}\|_{T\infty} \le \psi_{G2}$$

where

$$\begin{aligned}\psi_{G2} = \Big\| & \Delta\mathbf{c}_r\tilde{\boldsymbol{\theta}}_d(t) - \Delta\mathbf{G}_v\dot{\tilde{\boldsymbol{\theta}}}_d(t) + \mathbf{M}^{-1}(t)\tilde{\mathbf{M}}(t)\ddot{\boldsymbol{\theta}}_d(t-L) \\ & + \mathbf{M}^{-1}(t)(\tilde{\mathbf{Q}}_d(t) + \tilde{\mathbf{G}}(t) + \tilde{\mathbf{w}}(t)) + \Delta\mathbf{G}_v\mathbf{M}_s^{-1}\int_{t-L}^{t}\boldsymbol{\tau}_s(\sigma)d\sigma \\ & + \mathbf{M}^{-1}(t)\tilde{\boldsymbol{\tau}}_s(t)\Big\|_\infty + \delta_1\big(\eta_4\|\boldsymbol{\theta}_d(t)\|_{T\infty} + \gamma_4\|\boldsymbol{\tau}_s(t)\|_{T\infty} + \rho_4\big) \\ & + \delta_2\big(\eta_5\|\boldsymbol{\theta}_d(t)\|_{T\infty} + \gamma_5\|\boldsymbol{\tau}_s(t)\|_{T\infty} + \rho_5\big) \\ & + \delta_3\big(\eta_6\|\dot{\boldsymbol{\theta}}_d(t)\|_{T\infty} + \gamma_6\|\boldsymbol{\tau}_s(t)\|_{T\infty} + \rho_6\big) \\ & + \delta_4\big(\eta_1\|\boldsymbol{\theta}_d(t)\|_{T\infty} + \gamma_1\|\boldsymbol{\tau}_s(t)\|_{T\infty} + \rho_1\big) \\ & + \delta_5\big(\eta_2\|\dot{\boldsymbol{\theta}}_d(t)\|_{T\infty} + \gamma_2\|\boldsymbol{\tau}_s(t)\|_{T\infty} + \rho_2\big) \\ & + \delta_6\big(\eta_3\|\ddot{\boldsymbol{\theta}}_d(t)\|_{T\infty} + \gamma_3\|\boldsymbol{\tau}_s(t)\|_{T\infty} + \rho_3\big)\end{aligned} \quad (34)\square$$

*D. Sufficient Stability Condition for NBBIC*

We have shown the inequalities of $\|\boldsymbol{\varepsilon}(t)\|_{T\infty}$ by Lemma 2-1 and Lemma 2-2. The sufficient conditions for these inequalities to have upper bounds are shown below.

$$\mu + \delta_1\beta_4 + \delta_2\beta_5 + \delta_3\beta_6 + \delta_4\beta_1 + \delta_5\beta_2 + \delta_6\beta_3 < 1 \quad (35)$$

If (35) holds, $\|\boldsymbol{\varepsilon}(t)\|_{T\infty}$ has an upper bound because all terms of (35) are not related to *T*, which is a symbol of truncated norm. The fact that $\|\boldsymbol{\varepsilon}(t)\|_{T\infty}$ can have an upper bound means that the time-delay estimation error $\boldsymbol{\varepsilon}(t)$ of (18) can be bounded. Therefore, in the case of group 1 and group 2, stability can be guaranteed if we set control gains to satisfy (35). In the case of group 3, a robot is passive since there is no control input applied to it; hence, the system is stable [19] .Therefore, we can obtain the following stability theorem for the nonlinear bang-bang impact control from Lemma 1, 2-1 and 2-2.

***NBBIC Stability Theorem:*** The sufficient conditions for stability under the nonlinear bang-bang impact control become:

$$\mu + \delta_1\beta_4 + \delta_2\beta_5 + \delta_3\beta_6 + \delta_4\beta_1 + \delta_5\beta_2 + \delta_6\beta_3 < 1 \quad \square$$

*E. Physical Implication of NBBIC Stability Condition*

In order to understand the physical implication of NBBIC stability theorem, we substitute the norm values of (28) for free space case and of (34) for constrained space case into (35). Then we get,

$$\Big\|\big\|\mathbf{I} - \mathbf{M}^{-1}\bar{\mathbf{M}}\big\|_{i2}\Big\|_\infty < \frac{(1-c)}{1+(\beta_4\kappa_1 + \beta_5\kappa_2 + \beta_6\kappa_3)}, \quad (36)$$

where

$$\begin{aligned}\kappa_1 &= \|\mathbf{G}_v\mathbf{M}_s^{-1}\mathbf{K}_{des}\|_{i2} \\ \kappa_2 &= \|(\mathbf{G}_v\mathbf{M}_s^{-1}\mathbf{B}_{des} + \mathbf{K}_{des} - \mathbf{c}_r)\|_{i2} \\ \kappa_3 &= \|(\mathbf{G}_v + \mathbf{B}_{des})\|_{i2} \\ c &= \beta_5\Big\|\big\|\mathbf{M}^{-1}(t)\mathbf{q}_2(t)\big\|_{i2}\Big\|_\infty + \beta_6\Big\|\big\|\mathbf{M}^{-1}(t)\mathbf{q}_1(t)\big\|_{i2}\Big\|_\infty + \beta_1\Big\|\big\|\mathbf{M}^{-1}(t)\tilde{\mathbf{q}}_2(t)\big\|_{i2}\Big\|_\infty \\ &\quad + \beta_2\Big\|\big\|\mathbf{M}^{-1}(t)\tilde{\mathbf{q}}_1(t)\big\|_{i2}\Big\|_\infty + \beta_3\Big\|\big\|\mathbf{M}^{-1}(t)\tilde{\mathbf{M}}(t)\big\|_{i2}\Big\|_\infty .\end{aligned} \quad (37)$$

Note that $c$ in (37) is composed of the differences of bounded values such as $\tilde{\mathbf{M}}, \tilde{\mathbf{q}}_1$, and $\tilde{\mathbf{q}}_2$ and the bounded values multiplied by small values $\beta_5$ and $\beta_6$. Therefore, $c$ is negligible during the impact and constrained motion when there is not much change in Coriolis and centrifugal forces between time $t$ and $t$-$L$ [13], [15]. However, $c$ is not negligible during a certain constrained motion which involves significant changes in these state dependent forces between time $t$ and $t$-$L$.

When these terms are negligible, NBBIC is always stable if $\bar{\mathbf{M}} = \mathbf{M}$ since it makes the left hand side of (36) zero. In reality, however, it is difficult to estimate robot inertia $\mathbf{M}$ accurately. When the inertia estimate $\bar{\mathbf{M}}$ differs from the actual inertia$\mathbf{M}$, the stable range of $\bar{\mathbf{M}}$ is determined by the delay time $L$ and control gains. It can be deduced from (36)

[3] $\|\bullet(t-L)\|_{T\infty} \le \|\bullet(t)\|_{T\infty}$ [18]

that the more $\bar{\mathbf{M}}$ differs from $\mathbf{M}$, the smaller $L$ should be to achieve stability. It is noted that the system under NBBIC is stable regardless of controller gains if the estimation of inertia is accurate and a delay time $L$ is small. It is a natural conclusion because the NAC is designed to observe the passivity constraint. However, as the degrees of freedom of a robot increases, it becomes more difficult to obtain accurate estimation of robot inertia.

When there are significant changes in Coriolis and centrifugal forces between time $t$ and $t$-$L$, i.e., $c$ is not negligible as in free space and a certain constrained motion, it imposes more strict constraints on the range of $\bar{\mathbf{M}}$ and $L$. For example, if a robot under NBBIC approaches an environment from free space to perform a contact task on a fixed stiff wall, the stability condition for free space motion is more difficult to satisfy than that of such constrained motion. It was confirmed by experiments. Our experiments demonstrate that the nonlinear bang-bang impact controller can make stable contact with a stiff environment without changing gains by using gains set for stable free space motion [5], [6]. It shows that if the controller gains make stable free space motion, they can also make stable constrained space motion which experiences less change in Coriolis and centrifugal forces than those in free space.

## IV. Experiments

In this section, experiments are performed to verify the NBBIC stability theorem derived in Section III. The overall performances of the bang-bang impact controller are also demonstrated by experiments.

### A. Experiments for Stability Verification

Experiments are performed to verify the proposed stability criterion by using SCARA type two D.O.F. robot with sampling time $L$=1$ms$ (fig. 1 (a) ).

First, one D.O.F experiment is conducted using only the 2nd link of the robot. The objective is to drive robot 0.0746$m$ with desired velocity of 0.1865$m/s$, i.e., 0.0728$m$ in free space and 0.0018$m$ after contact with silicon wall. The theoretical stable range of the inertia estimate $\bar{M}$ is $0.0284 kg{\cdot}m^2 \le \bar{M} \le 0.0371 kg{\cdot}m^2$ with $M_s$=0.12 $kg{\cdot}m^2$, $G_v$=12 $N{\cdot}s{\cdot}m$, $B_{des}$=30 $N{\cdot}s{\cdot}m$, and $K_{des}$=140 $N{\cdot}m$. The experimental results in fig.2 show that stable response is obtained with lower stability bound. But, the stable upper bound of $\bar{M}$ is observed to be 0.036 $kg{\cdot}m^2$. Second, two D.O.F. experiments are performed with the same stable gains used for the one D.O.F. experiments. $\bar{\mathbf{M}}$ is selected as a constant diagonal matrix ($diag[\alpha_1, \alpha_2]$) and the maximum stable gain of $\alpha_2$=0.030 $kg{\cdot}m^2$ is used. With these values, the theoretical stable range of $\alpha_1$ is $0.32 kg{\cdot}m^2 \le \alpha_1 \le 0.61 kg{\cdot}m^2$. The lower bound of 0.32 $kg{\cdot}m^2$ produces stable response as shown in fig.3. However, it is observed that the maximum stable upper bound is 0.5 $kg{\cdot}m^2$ instead of 0.61 $kg{\cdot}m^2$.

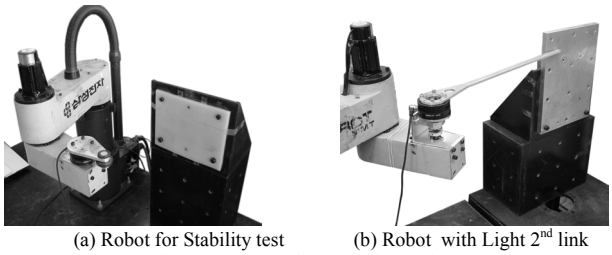

(a) Robot for Stability test (b) Robot with Light 2nd link

Fig 1. SCARA Robot Experimental setup

It appears that the stable upper bound is limited by noise effect due to acceleration signals and etc. If we employ a first order digital low pass filter with the cutoff frequency $\lambda$ to cancel noise, control input changes accordingly as below [20].

$$\boldsymbol{\tau}'(t) = \bar{\mathbf{M}}\left(\mathbf{u}(t) - \ddot{\boldsymbol{\theta}}(t-L)\right) + \boldsymbol{\tau}(t-L), \tag{38}$$

$$\boldsymbol{\tau}(t) = \frac{\lambda'}{1+\lambda'}\boldsymbol{\tau}'(t) + \frac{1}{1+\lambda'}\boldsymbol{\tau}(t-L) \qquad (\lambda' = \lambda L), \tag{39}$$

where $\boldsymbol{\tau}'$ is the input to the filter and $\boldsymbol{\tau}$ is the output from the filter. Substituting (38) into (39) leads to the following control input.

$$\boldsymbol{\tau}(t) = \frac{\lambda'}{1+\lambda'}\bar{\mathbf{M}}\left(\mathbf{u}(t) - \ddot{\boldsymbol{\theta}}(t-L)\right) + \boldsymbol{\tau}(t-L) \tag{40}$$

Thus the use of a first order digital low pass filter has the same effect as lowering of $\bar{\mathbf{M}}$. The noise effect is more pronounced with higher gains of $\bar{\mathbf{M}}$ since they excite high frequency dynamics of robots. That is the reason why the stable upper bound is lower than the theoretical one.

### B. Experiments for Control Performance Comparison

This section demonstrates the overall performances of the NBBIC. For the experiments, the second link of the SCARA robot of fig.1 (a) is replaced by a light-weight link of fig. 1

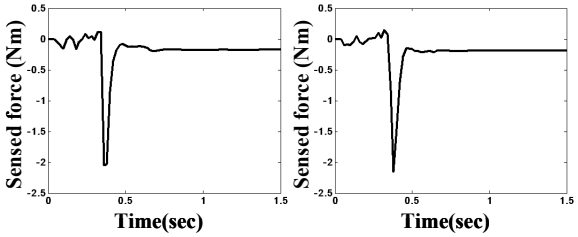


(a) $\bar{M} = 0.0284\ \mathrm{kg \cdot m^2}$ (b) $\bar{M} = 0.036\ \mathrm{kg \cdot m^2}$

Fig. 2. Contact force (one D.O.F)

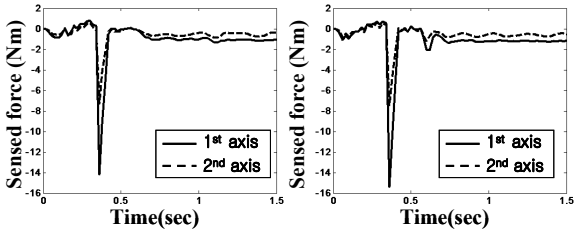


(a) $\alpha_1 = 0.32\ \mathrm{kg \cdot m^2}$ (b) $\alpha_1 = 0.5\ \mathrm{kg \cdot m^2}$

Fig. 3. Contact force (two D.O.F)

(b) due to the limited range of force sensor. The environment is a thick aluminum plate. The new robot link is attached to an ATI Gamma SI-130-10, 10Nm range, force sensor. The other side of force sensor is coupled to a Maxonmotor Planetary gear 203119(gear ratio of 26:1) via a coupling. The gear is attached to a Maxon Precision Motors DC motor 148877, which is connected to a Hewlett Packard HEDL-9140 3 channel incremental industrial encoder with a resolution of 500 counts-per-revolution with quadrature output.

First, impact performance test is carried out. The experiment has three stages of motion: free space motion, impact, and constrained motion. The robot hits the environment with the impact velocity of 1.5 *m/sec* while control parameters are adjusted to produce the best stable performance against the aluminum wall**.** Fig.4 shows impact control results. The robot experiences an impact force of approximately 5.5 *Nm* and the settling time is 0.24 *sec*.

For a soft environment such as silicon wall ( fig. 4 (b) ), the control performance was almost same as that for a stiff environment like steel wall as shown in fig. 4. (c). The same control gains are used for aluminum, silicon, and steel wall. Thus, our experiments demonstrate that bang-bang impact control is robust to environmental change for a wide range of gains making it attractive in an unstructured environment. It confirms the stability condition that stability does not depend on environments. We observe that the impact control performance depends on operating conditions, such as humidity and temperature, which affect friction at robot joints.

Next, the NBBIC performs a seamless contact manipulation that involves impact with only one control algorithm and the same gains in all three contact modes as shown in fig. 4 (d). An experiment was performed to demonstrate this advantage. First, the robot arm was commanded to travel toward an aluminum plate fixed on the wall and hit the plate with impact velocity of 1.5 *m/s*. After the robot reaches the steady state, the second link of the robot was moved back and forth repeatedly by a hollow aluminum stick while the robot link kept contact with the stick. For NAC/TDC, the control parameters remained the same throughout the experiment. Our experiments show that the gains for stable free motion also create a stable contact with the aluminum plate. Fig 4 shows that the one-link arm quickly absorbs impact energy and then performs a stable contact task.

Lastly, we investigate disturbance rejection property of NBBIC in free space using the same control gains as in the impact experiments. We manually applied a sudden torque of approximately 3.5 *Nm* ( fig. 5 (a) ) by using a hollow aluminum stick to the second link of the robot while it is following a sinusoidal trajectory. Control gains remain the same throughout the operation. It is observed that the robot keeps its trajectory successfully despite of the pulse disturbance as shown in fig. 5. It indicates that NBBIC can ignore minor disturbance while it tries to accomplish a certain task in free space. It is also observed that NBBIC excels in trajectory following in free space among other impact control techniques [7].

The experimental results show that the NBBIC is effective in subsiding impact oscillations, following desired trajectory even under a sudden disturbance, and constrained motion without changing control gains [7].

## V. CONCLUSION

In this paper, we derived sufficient stability conditions for the nonlinear bang-bang impact control based on $L_\infty^n$ space analysis. The stability condition has a concise form and gives straightforward physical insight. The analysis shows that when the inertia estimate $\bar{\mathbf{M}}$ differs from the actual inertia $\mathbf{M}$, the stable range of $\bar{\mathbf{M}}$ is determined by a delay time $L$ and control gains. It also shows that it is more difficult to achieve stability in free space than in a certain constrained motion, which does not involve significant changes in Coriolis and centrifugal forces between time $t$ and $t$-$L$. Experimental results validate the sufficient stability conditions. In reality, however, experimental noises reduce the stability region and it is more apparent as the order of systems increases.

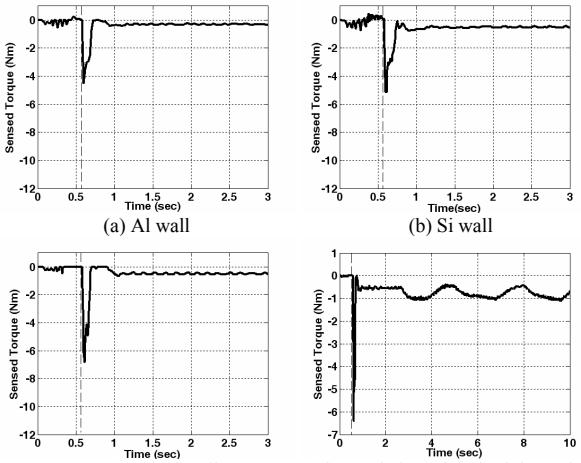


(a) Al wall (b) Si wall

(c) Steel wall (d) Emulation of desired dynamics

Fig.4. Impact and constrained motion results (Dashed line indicates impact time)

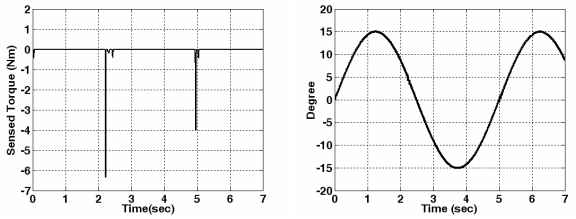


a) Disturbance torque ( NBBIC ) (b) Position under NBBIC

Fig.5 Experiment in free space

The experimental results for a multi-degree of freedom robot show that the simple NBBIC demonstrates excellent performances in all three modes of free space, impact, and constrained motion without changing control gains.

NBBIC can be used for robot interactions with unknown physical environments such as robots in space exploration, cooperative robot tasks and mobile robots. NBBIC can also be used for micro/nano manipulations using an atomic force microscope, where real time vision is unavailable during contact manipulation without an additional vision system.

## APPENDIX

In (27) $\mathbf{q_1}(t)$ can be expressed as following.

$$\mathbf{q_1}(t) = \mathbf{p}_1(t) + \mathbf{p}_2(t)\dot{\mathbf{e}}(t) \tag{41}$$

where $\mathbf{p}_1(t)$ , $\mathbf{p}_2(t)$ are bounded functions of time. Substituting (33) of lemma 2-1 into (21) of lemma 1 and using (41), we can get the following.

$$\begin{aligned}\left\|\dot{\mathbf{e}}\right\|_{T\infty} \le & \frac{\beta_2 \psi_{G1}}{\left(1-\mu-\delta_1\beta_4-\delta_2\beta_5-\beta_6 P_a\left\|\dot{\mathbf{e}}\right\|_{T\infty}-\delta_4\beta_1-\beta_2 P_b\left\|\dot{\mathbf{e}}\right\|_{T\infty}-\delta_6\beta_3-P_c\right)} \\ & +\gamma_2\left\|\boldsymbol{\tau}_s\right\|_{T\infty}+\eta_2\left\|\dot{\boldsymbol{\theta}}_d\right\|_{T\infty}+\rho_2\end{aligned} \tag{42}$$

where

$$\begin{aligned} P_a &= \left\|\left\|\mathbf{M}^{-1}(t)\mathbf{p}_2(t)\right\|_{i2}\right\|_\infty \\ P_b &= 3\left\|\left\|\mathbf{p}_2(t)\right\|_{i2}\right\|_\infty \\ P_c &= \beta_6\left\|\left\|\boldsymbol{\Delta}\left(\mathbf{G}_v+\mathbf{B}_{des}\right)+\mathbf{M}^{-1}(t)\mathbf{p}_1(t)\right\|_{i2}\right\|_\infty \\ &\quad +\beta_2\left\|\left\|\mathbf{M}^{-1}(t)\tilde{\mathbf{p}}_1(t)\right\|_{i2}\right\|_\infty \end{aligned} \tag{43}$$

Therefore, the velocity error can be guaranteed to be bounded within the set *S*. It can be also shown that the position error can be bounded by using similar method.

## REFERENCES


[1] W.L. Xu, J.D. Han, S.K. Tso, "Experimental study of contact transition control incorporating joint acceleration feedback," *IEEE/ASME Trans. On Mechatronics*, vol. 5, pp.292-301, Sept. 2000.

[2] D.N. Nenchev, K.Yoshida, "Impact analysis and post-impact motion control issues of a free-floating space robot subject to a force impulse," *IEEE Trans. on Robotics and Automation*, vol. 15, pp.548-557, June 1999.

[3] M. Indri and A. Tornambe, "Impact model and control of two multi-DOF cooperating manipulators," *IEEE Trans. on Automat. Contr.*, vol.44, no 6, pp. 1528-1533, June 1999.

[4] E. Lee, "Force and impact control for robot manipulators with unknown dynamics and disturbances," Ph.D. Dissertation, Dept. of Mechanical and Aerospace Engineering, Case Western Reserve Univ., Cleveland, OH, August, 1994.

[5] E. Lee, J. Park, C.B. Schrader, and P.H. Chang, "Hybrid impedance/time-delay control from free space to constrained motion," in *Proc. of American Control Conference*, Denver, CO, June 2003, pp.2132-2137.

[6] E. Lee, J. Park, K. A. Loparo, C.B. Schrader, and P. H. Chang, "Bang-Bang impact control using hybrid impedance/time-delay control," *IEEE/ASME Trans. on Mechatronics*, vol.8, no. 2, pp.272-277, June 2003.

[7] S. H. Kang, M. Jin, P. H. Chang, and E. Lee, "Robot interaction control in unstructured space environment for space exploration," in *Proc. of AIAA unmanned unlimited technical conference*, Chicago, IL, Sept. 2004.

[8] W. S. Newman, "Stability and performance limits of interaction controllers," *Trans. of ASME, J. Dyn. Sys., Meas., Contr.*, vol.114, pp.563-570, 1992.

[9] K. Youcef-Toumi and O. Ito,"A time delay controller for systems with unknown dynamics," *Trans. of ASME, J. Dyn. Sys., Meas., Contr.*, vol. 112, pp133-142, 1990.

[10] T. C. Hsia and L. S. Gao, "Robot manipulator control using decentralized linear time-invariant time delayed joint controllers," in *Proc. of IEEE Int. Conf. on Robotics and Automation*, Cincinnati, Ohio, May 1990, pp. 2070-2075.

[11] A. Chatterjee, "A new algebraic rigid body collision based on impulse space considerations," *Trans. of ASME. J. Applied Mechanics*, vol. 65, no.4, pp.939-951, 1998.

[12] K. Youcef-Toumi, and D.A. Gutz, "Impact and force control: modeling and experiments," *ASME J. of Dyn, Sys., Meas., Contr.*, vol. 116, pp.89-98, 1994.

[13] I. D. Walker, "Impact configurations and measures for kinematically redundant and multiple armed robot systems," *IEEE Trans. on Robotics and Automation*, vol.10, no.5, pp.670-683, Oct. 1994.

[14] J. K. Mills, and C. V. Nguyen, "Robotic manipulator collisions: modeling and simulations," *Trans. Of ASME J. Dyn, Sys., Meas., Contr.*, vol.114, pp. 650-659, 1992.

[15] P. R. Pagilla, and B. Yu, "A stable transition controller for constrained robots," *IEEE/ASME Trans. on Mechatronics*, vol.6, pp.65-74, Mar. 2001.

[16] M. W. Spong and M. Vidyasagar, "Robust linear compensator design for nonlinear robotic control," *IEEE J. of Robotics and Automation*, vol.RA-3, no.4, pp.345-351, Aug. 1987.

[17] J. H. Jung, P. H. Chang, O. S. Kwon, " A new stability analysis of time delay control for input-output linearizable plants," in *Proc. of American Control Conference*, Boston, MA, June 2004, pp.4972-4979.

[18] H. K. Khalil, *Nonlinear systems*, Prentice Hall, 2nd edition, 1996.

[19] R. Ortega and M. W. Spong, "Adaptive motion control or rigid robots: A tutorial," in *Proc. of IEEE Int. Conf. on Decision and Control*, Dec. 1988, pp. 1575-1584.

[20] K. Youcef-Toumi and S.-T. Wu, "Input/Output linearization using time delay control," *Trans. of ASME, J. Dyn, Sys., Meas., Contr*, vol. 114, pp. 10-19, 1992.